Article

Anionic and Magnetic Ordering in Rare Earth Tantalum Oxynitrides with an *n* = 1 Ruddlesden−Popper Structure

Published as part of the Chemistry of Materials virtual special issue "C. N. R. Rao at 90".

Jhonatan R. Guarín, Carlos Frontera, Judith Oró-Solé, Bastian Colombel, Clemens Ritter, François Fauth, Josep Fontcuberta,* and Amparo Fuertes*

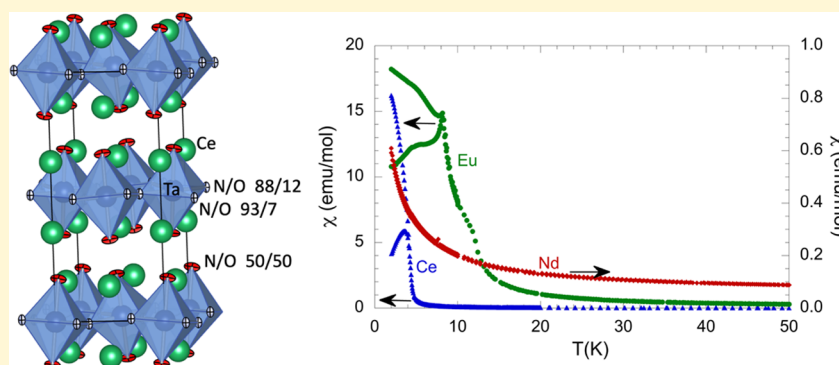Cite This: *Chem. Mater.* 2024, 36, 5160−5171

Read Online

ACCESS | Metrics & More | Article Recommendations | SI Supporting Information

ABSTRACT: The new compounds $R_2TaO_{4-x}N_x$ with R = La, Ce, Nd, and Eu and $1.20 \leq x \leq 2.81$ have been obtained by a solid-state reaction between metal nitrides and oxides or oxynitrides under N_2 gas at temperatures between 1200 and 1700 °C. They are the first examples of rare earth transition metal oxynitrides with an *n* = 1 Ruddlesden−Popper structure and show different anion stoichiometries, crystal structures, and magnetic properties. Synchrotron X-ray powder diffraction and electron diffraction indicate that the lanthanum, cerium, and neodymium compounds crystallize in the orthorhombic space group *Pccn*, with cell parameters *a* = 5.72949(2), *b* = 5.73055(5), and *c* = 12.77917(6) Å for $La_2TaO_{1.31}N_{2.69}$, *a* = 5.70500(5), *b* = 5.71182(4), and *c* = 12.61280(7) Å for $Ce_2TaO_{1.19}N_{2.81}$, and *a* = 5.70466(3), *b* = 5.70476(5), and *c* = 12.32365(5) Å for $Nd_2TaO_{1.46}N_{2.54}$. In contrast, $Eu_2TaO_{2.80}N_{1.20}$ shows a tetragonal $I4_1/acd$ superstructure doubling the *c* axis, with parameters *a* = 5.71867(2) and *c* = 25.00092(19) Å. Refinement of neutron powder diffraction data of $Ce_2TaO_{1.19}N_{2.81}$ indicated the nitrogen order in the two equatorial positions of the tantalum octahedron, with refined N/O occupancies of 0.930(7)/0.070 and 0.876(13)/0.124, and the axial position is occupied by 50% of each anion. This anion ordering agrees with the distribution predicted by Pauling's second crystal rule. Magnetization measurements show that the cerium and europium compounds are ordered magnetically at low temperatures, while the neodymium compound remains paramagnetic down to 2 K, as a consequence of suppression of the effective magnetic moment of the latter when reducing the temperature.

INTRODUCTION

Perovskite oxynitrides have been widely investigated in the last two decades because of their notable applications as electronic and photocatalytic materials. The strategy for finding new properties is based on the lower electronegativity of nitrogen compared to that of oxygen, which induces changes in the electronic structures and increases the covalency of bonds with the metals. Additionally, the larger electrical charge of the anion N^{3-} compared to O^{2-} allows the formation of phases with new combinations of cations that show oxidation states different than in the analogous oxides. The majority of known compounds are pseudocubic simple perovskites derived from the $Pm\bar{3}m$ aristotype, of the general formula $ABO_{3-x}N_x$ with A = alkaline earth or rare earth metal and B = early transition metal, showing
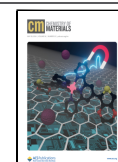
different crystal symmetries induced by octahedral tilting and the anion order.[1] Important examples of materials are nontoxic pigments $La_{1-x}Ca_xTaO_{1+x}N_{2-x}$,[2] $EuNbO_2N$ and $EuWO_{1+x}N_{2-x}$ with colossal magnetoresistance at low temperatures,[3,4] $BaTaO_2N$ and $SrTaO_2N$ with high dielectric constants,[5] and

several tantalum perovskites with photocatalytic activity in water splitting.[6,7]

There are few reported perovskite oxynitrides with complex structures. Examples of double and triple perovskites are $Sr_2FeMoO_{4.9}N_{1.1}$,[8] Sr_2FeWO_5N,[9] La_2MnTaO_5N,[10] and $Eu_3Ta_3O_{3.66}N_{5.34}$,[11] all of them showing magnetic ordering at low temperatures. Polar $BaWON_2$ is the only known example of a hexagonal perovskite.[12] Layered, Ruddlesden–Popper[13] perovskite oxynitrides $(AX)(ABX_3)_n$ (X = O, N) were first reported by R.Marchand and co-workers for the $n = 1$ members Sr_2TaO_3N, Ba_2TaO_3N,[14] and R_2AlO_3N (R = La, Nd, Sm).[15] We prepared the $n = 1$ and 2 members of the series (SrO)-$(SrNbO_2N)_n$, with the compositions Sr_2NbO_3N and $Sr_3Nb_2O_5N_2$, respectively,[16] and the $n = 2$ compound $Eu_3Ta_2O_3N_4$ has been recently reported.[17]

Rare earth perovskite oxynitrides are known for the transition metals Cr, Ti, Zr, Hf, V, Nb, Ta, and W, and they have been mostly investigated for their electronic and photocatalytic properties. $RCrO_{3-x}N_x$ (R = La, Pr, and Nd) perovskites show antiferromagnetic coupling of Cr^{3+}/Cr^{4+} spins with Neel temperatures from 285 to 214 K.[18] Vanadium perovskites with R = La and Pr show spin freezing transitions at low temperatures.[19] $EuTaO_2N$, $EuNbO_2N$,[3] and $EuWO_{1+x}N_{2-x}$[4] are ferromagnetic with T_c values between 5 and 12 K because of Eu^{2+} spin ordering. $LaTiO_2N$[20] and $RHfO_2N$[21] (R = La, Nd, Sm) compounds are visible light-active photocatalysts in water oxidation and reduction, whereas $LaTaON_2$, in addition to a photocatalyst for water splitting,[22] is a high-dielectric permittivity material.[23]

In this paper, we report the synthesis, crystal structures, and magnetic properties of the new compounds $R_2TaO_{4-x}N_x$ (R = La, Ce, Nd, and Eu) that are the first examples of transition metal $n = 1$ Ruddlesden–Popper oxynitrides with a rare earth cation at the A sites. These oxynitrides can be stabilized by using a high-temperature synthesis method under N_2, starting with a mixture of metal nitrides and oxides. The obtained anion stoichiometries indicate reduction of the cations during synthesis and are determined by the stable oxidation states of tantalum (Ta^{4+}, Ta^{5+}) and the rare earth cations (La^{3+}, Ce^{3+}, Nd^{3+}, and Eu^{2+}/Eu^{3+}) under the preparative conditions. The anion distribution is investigated by neutron diffraction for $Ce_2TaO_{1.19}N_{2.81}$, showing the order of nitrides at the equatorial sites of the octahedra, whereas the axial positions are occupied by 50% of each anion. The cerium and europium compounds develop low-temperature (<10 K) magnetic ordering, while the Nd compound is paramagnetic down to 2 K. The striking differences between the magnetic behaviors of the Ce^{3+}, Nd^{3+}, and Eu^{2+}/Eu^{3+} compounds are rationalized in terms of the distinct role that crystal field effects and exchange interactions play in determining the singlet or triplet ground state of the rare earth cations.

■ EXPERIMENTAL METHODS

Synthesis and Chemical Characterization. Samples of 100 to 200 mg of $R_2TaO_{4-x}N_x$ (R = La, Ce, Nd, Eu) compounds were prepared by a solid-state reaction under N_2 gas (Air Liquide, 99.9999%) at temperatures between 1200 and 1700 °C, starting from mixtures with different proportions of RN, R_2O_3, Ta_3N_5, and TaON, while keeping the stoichiometric ratio R/Ta of 2:1. $La_2TaO_{1.31}N_{2.69}$ was prepared starting with LaN and Ta_3N_5 (Alfa Aesar 99.9%) in a molar ratio of 6:1 at 1700 °C, $Ce_2TaO_{1.19}N_{2.81}$ was prepared from CeN, Ta_3N_5, and TaON in a molar ratio of 6:0.375:1.875 at 1500 °C, $Nd_2TaO_{1.46}N_{2.54}$ was prepared from Nd_2O_3(Aldrich 99.99%), NdN (Alfa Aesar 99.9%), and Ta_3N_5 at 1500 °C with a ratio of 0.05:1.9:0.33, and $Eu_2TaO_{2.80}N_{1.20}$

was obtained from Eu_2O_3 (Sigma-Aldrich 99.9%), EuN (Materion, 99.9%), and Ta_3N_5 in a ratio of 0.85:0.30:0.33 at 1200 °C. The proportion of the reactants determining the O/N ratio in the initial mixture and the maximum synthesis temperature were optimized from several syntheses performed for each compound, until the sample was a single phase from laboratory X-ray diffraction. CeN was obtained by treatment under N_2 of Ce chips (Strem 99.9%) at 1000 °C. Ta_3N_5 was obtained from Ta_2O_5 (Sigma-Aldrich 99.99%) by treatment under NH_3 (Carburos Metálicos 99.9%) at 880 °C using a flow rate of 600 cm^3/min and several treatments of 15 h with intermediate regrinding. TaON was prepared by a similar procedure but using a flow rate of 40 cm^3/min and two treatments of 3 h with intermediate regrinding. Nd_2O_3 and Eu_2O_3 were treated at 900 °C under a dynamic vacuum of 1×10^{-3} Torr for dehydration. Handling, mixing, and pelletizing of the reactants were performed inside a glovebox under recirculating Ar. The samples were placed in molybdenum crucibles covered by Zr foil that was also placed in a second molybdenum crucible in order to scavenge oxygen and water from the N_2 gas. The reaction tube was evacuated to 10^{-3} Torr and purged several times with N_2 before starting the thermal cycle. This consisted of a single treatment of heating at 300 °C/h up to the maximum temperature that was kept for 3 h, with further natural cooling to room temperature.

Nitrogen contents were determined by combustion analysis performed in a Thermo Fisher Scientific instrument, heating the samples in oxygen up to 1060 °C and using MgO, WO_3, and Sn as additives and atropine as a reference standard. EDX analyses of cation contents were performed in a FEI Quanta 200 FEG microscope equipped with an EDAX detector with an energy resolution of 132 eV. The analyses were performed on 10−15 crystallites for each sample.

Structural Characterization. Laboratory powder X-ray diffraction was used for controlling the purity of the samples during the synthesis. Data were acquired on a Panalytical X'Pert Pro MPD diffractometer using Cu Kα radiation (λ = 1.5418 Å) and on a Bruker D8 Advance A25 diffractometer in a Debye−Scherrer configuration with Mo Kα_1 radiation (λ = 0.7093 Å) using capillary samples (0.3 mm diameter). High-angular resolution synchrotron X-ray powder diffraction data were collected at room temperature from capillary samples in the angular range of $2.0° \leq 2\theta \leq 56.9°$ at the MSPD beamline[24] of the ALBA Synchrotron (Cerdanyola del Vallès, Spain), using 30 keV energy that resulted in exact wavelengths of 0.4137, 0.4139 and 0.4142 Å as determined by refining the SRM640d NIST Si standard. Neutron powder diffraction was used to determine the anion distribution in $Ce_2TaO_{1.19}N_{2.81}$. Data on a 80 mg sample were collected for 19 h at room temperature on the high-intensity D20 diffractometer at the Institut Laue-Langevin (ILL), France, using a vanadium can as a sample holder. The pattern was measured in scanning mode with a short wavelength of 1.37 Å created by using 118° takeoff angle, giving high resolution. Rietveld analysis was carried out using the program Fullprof.[25] Background refinement was performed by linear interpolation, and data were corrected from absorption.
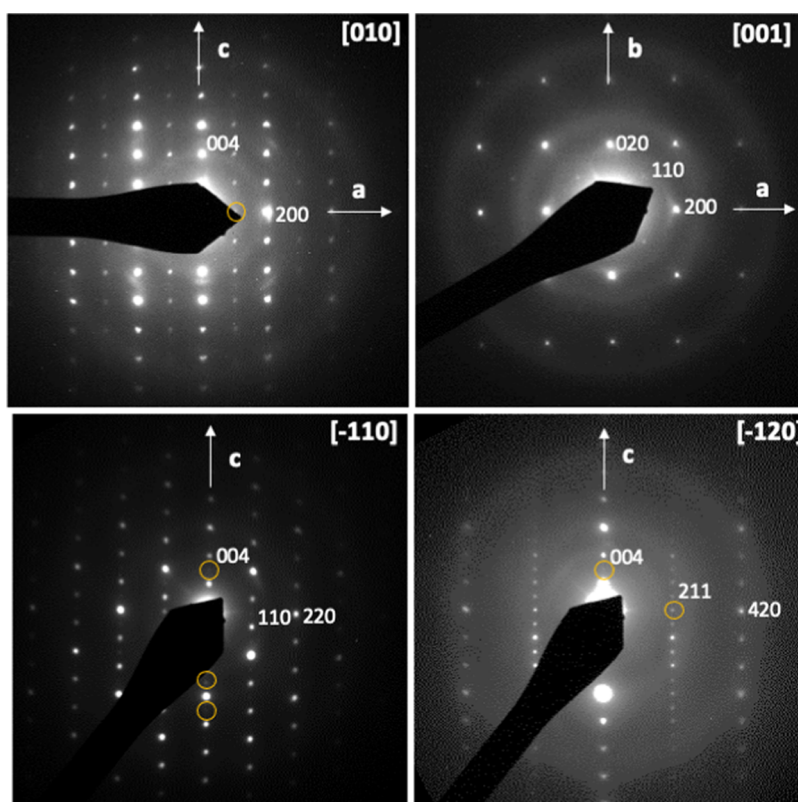
Electron diffraction micrographs were obtained in a JEOL 1210 transmission electron microscope operating at 120 kV using a side entry double tilt ±60°/±30° specimen holder. The samples were prepared by depositing the powder on a copper grid coated with a holey carbon film.

Magnetic Measurements. Magnetic measurements were performed at fields of 25 and 10 kOe between 2 and 300 K using a Quantum Design SQUID magnetometer. Magnetization field loops were measured between −70 and +70 kOe between 2 and 16 K.

■ RESULTS AND DISCUSSION

Synthesis and Crystal Structures of $R_2TaO_{4-x}N_x$ Compounds. The synthesis of new rare earth tantalum $n = 1$ Ruddlesden−Popper compounds was performed using the reactions at high temperature under N_2

$$(3 - y)R_2O_3 + 2yRN + Ta_3N_5 \rightarrow 3R_2TaO_{4-x}N_x \text{ for R}$$
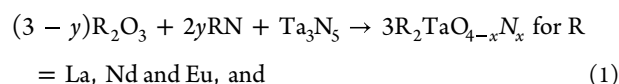
$$= \text{La, Nd and Eu, and} \qquad (1)$$

Figure 1. Selected electron diffraction patterns of $Ce_2TaO_{1.19}N_{2.81}$. Yellow circles indicate multiple diffraction reflections.

$$2RN + 1/8Ta_3N_5 + 5/8TaON \rightarrow R_2TaO_{4-x}N_x \text{ for } R$$
$$= Ce \qquad (2)$$
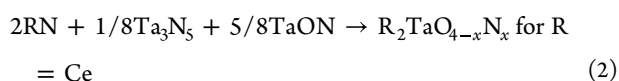
The best samples of La, Nd, and Eu were obtained for $y = 3$, 2.85, and 0.45, respectively. In the case of cerium, we used TaON as an oxygen source because Ce_2O_3 is not easily available commercially. This synthetic route is similar to that used for the preparation of the rare earth perovskites $LaTaON_2$,[23] $EuTaO_{2.37}N_{0.63}$, and $Eu_3Ta_3O_{3.66}N_{5.34}$[11] that we have recently reported and produces samples of high crystallinity with short reaction times. The rare earth perovskite oxynitrides are commonly prepared under NH_3 at temperatures below 1000 °C, starting with oxide precursors such as scheelites because the rare earth binary oxides are poorly reactive in these conditions.[26] R_2O_3 reactants have been used for the synthesis of few compounds under NH_3 but in the presence of fused salts that increase the kinetics of the nitridation[27] or in high-pressure conditions.[28] The combination of rare earth nitrides, RN, with different proportions of oxides and nitrides allows one to change the nitrogen/oxygen ratio in the initial mixture up to avoiding or minimizing the impurity phases. These are frequently formed in the synthesis of nitrides at high temperatures because of the presence of oxygen or water around the sample.

The black-colored $R_2TaO_{4-x}N_x$ samples were prepared at different temperatures optimized in each case, from 1200 °C for R = Eu to 1700 °C for R = La, and showed analyzed nitrogen contents of 2.69(3), 2.81(3), 2.54(3), and 1.20(3) atoms per formula for R = La, Ce, Nd, and Eu, respectively. In all cases, these contents were below the nitrogen stoichiometry in the mixture of reactants (3, 3.25, 3.56, and 1.96 for La, Ce, Nd, and Eu samples, respectively), indicating the incorporation of extra oxygen in the samples during synthesis. Nitrogen loss at high temperatures has been observed in other tantalum perovskites

such as $SrTaO_2N$[29] and $LaTaON_2$[23] and has been interpreted as a decomposition reaction releasing N_2 with partial reduction of Ta^{5+} to Ta^{4+}, analogous to the oxygen loss of transition metal oxides at high temperatures that produces reduced oxides together with O_2.[30] The corresponding cation ratios determined by EDX were La/Ta = 1.82(17), Ce/Ta = 1.81(10), Nd/Ta = 1.77(17), and Eu/Ta = 1.89(15), which agree with the nominal compositions within the experimental error. The oxygen stoichiometries were calculated by difference, assuming that the total anion content was four atoms per formula, resulting in $La_2TaO_{1.31}N_{2.69}$, $Ce_2TaO_{1.19}N_{2.81}$, $Nd_2TaO_{1.46}N_{2.54}$, and $Eu_2TaO_{2.80}N_{1.20}$. Considering charge compensation and the trivalent oxidation state for the rare earth cations, the nitrogen deficiency with respect to the ideal R_2TaON_3 composition in the La, Ce, and Nd compounds would result in a proportion of Ta^{4+} of 31, 19, and 46%, respectively. Compared with the other rare earth compounds, the observed N content in $Eu_2TaO_{2.80}N_{1.20}$ indicates that europium is dominantly divalent, which is consistent with the observed structural data and the magnetic properties (see below). In the synchrotron X-ray powder diffraction patterns of lanthanum, neodymium, and europium samples, we detected the perovskite-phase $RTaON_2$ with the respective amounts of 6.6, 5.1, and 1.9% (w/w) as determined from Rietveld refinement.

The electron diffraction patterns of the compounds $La_2TaO_{1.31}N_{2.69}$, $Ce_2TaO_{1.19}N_{2.81}$, and $Nd_2TaO_{1.46}N_{2.54}$ showed additional reflections to those expected for the $I4/mmm$ space group of the K_2NiF_4 aristotype (see Figures 1, S1, and S2) indicative of a tilted superstructure with parameters $\sqrt{2}a_0 \times \sqrt{2}a_0 \times c_0$ (where a_0 and c_0 are the parameters of the $I4/mmm$ cell). The reconstruction of the reciprocal lattice led to an orthorhombic cell with parameters a, $b \simeq 5.7$ Å and the respective c axis of 12.89, 12.60, and 12.53 Å for R = La, Ce, and
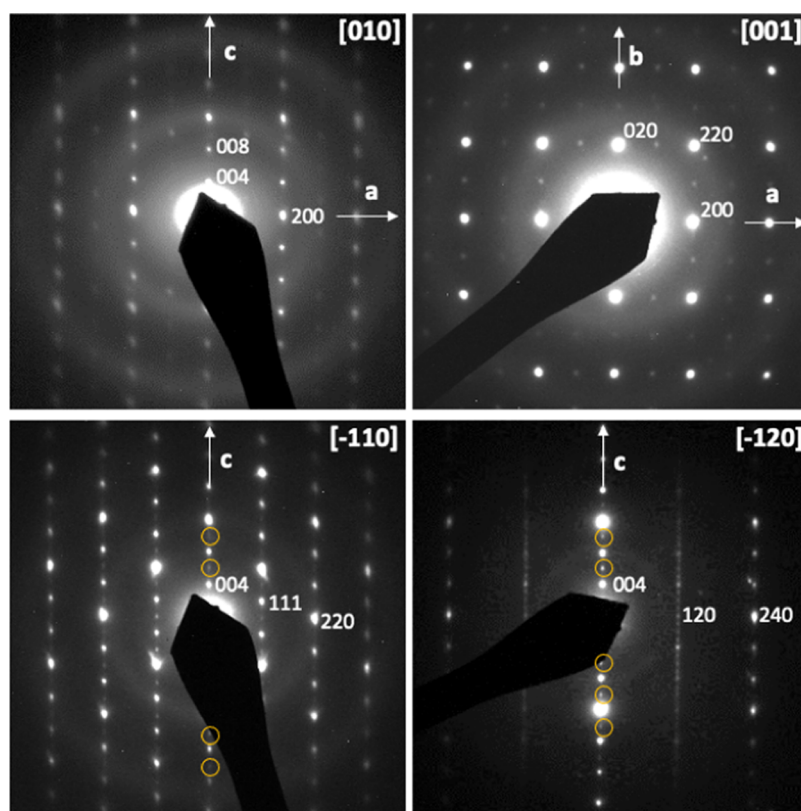
Figure 2. Selected electron diffraction patterns of $Eu_2TaO_{2.80}N_{1.20}$ with reflections indexed in the tetragonal cell with $a \simeq 5.7$ and $c \simeq 25$ Å. Yellow circles indicate multiple diffraction reflections.

Nd, with the observed reflection conditions consistent with the space group $Pccn$ (No. 56) ($hk0, h+k = 2n$; $h0l, l = 2n$; $0kl, l = 2n$; $h00, h = 2n$; $0k0, k = 2n$; $00l, l = 2n$). This space group corresponds to a tilted $n = 1$ Ruddlesden−Popper structure with out-of-phase rotations around the a and b axis, notated as $\phi_1 \phi_2 0$ for the first layer of octahedra and $\phi_2 \phi_1 0$ for the second layer of octahedra at the origin and body center of the $I4/mmm$ parent cell, and no rotation around the c axis.[31,32] In contrast, the compound $Eu_2TaO_{2.80}N_{1.20}$ showed an additional superstructure along the c axis doubling c_0, with cell parameters $a = 5.72$ Å and $c = 24.99$ Å (Figure 2). The electron diffraction planes indicated reflection conditions compatible with the space group $I4_1/acd$, which has been reported for K_2NiF_4 compounds including Sr_2IrO_4.[33] Weak additional reflections were also observed that could be indexed in a larger cell, with $a = 8.15$ Å and $c = 24.99$ Å.

Rietveld refinement of synchrotron X-ray diffraction data was performed in the $Pccn$ space group for the La, Ce, and Nd compounds (Figures 3, 4, and 5 and Tables 1, 2, and S1, respectively) and led the cell parameters $a = 5.72949(2)$, $b = 5.73055(5)$, and $c = 12.77917(6)$ Å for $La_2TaO_{1.31}N_{2.69}$, $a = 5.70500(5)$, $b = 5.71182(4)$, and $c = 12.61280(7)$ Å for $Ce_2TaO_{1.19}N_{2.81}$, and $a = 5.70466(3)$, $b = 5.70475(5)$, and $c = 12.32365(5)$ Å for $Nd_2TaO_{1.46}N_{2.54}$. For the refinement of the La and Nd compounds, we fixed a statistical distribution of nitrogen and oxygen in the three available anion sites because the X-rays do not provide enough contrast between the two anions. For $Ce_2TaO_{1.19}N_{2.81}$, we used and fixed the occupancies obtained from the refinement of neutron diffraction data (see the next section). The structural model of this compound is shown in Figure 6.
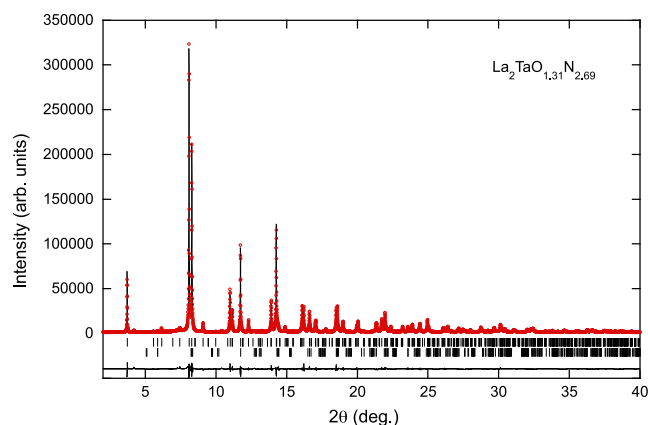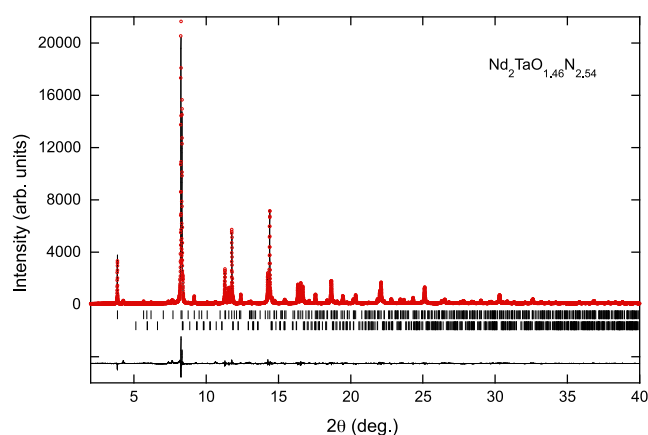

Figure 3. Rietveld fit to the synchrotron X-ray powder diffraction pattern of $La_2TaO_{1.31}N_{2.69}$ performed in the space group $Pccn$ with parameters $a = 5.72949(2)$, $b = 5.73055(5)$, and $c = 12.77917(6)$ Å. Upper and lower reflection markers are, respectively, for $La_2TaO_{1.31}N_{2.69}$ and $LaTaON_2$.[23]

The refinement of the crystal structure of $Eu_2TaO_{2.80}N_{1.20}$ from synchrotron X-ray diffraction data was performed in the space group $I4_1/acd$ starting with the atomic coordinates of Sr_2IrO_4[33] and led to the cell parameters $a = 5.71867(2)$ and $25.00092(19)$ Å ($\sqrt{2}a_0 \times \sqrt{2}a_0 \times 2c_0$) (Figures 7 and 8, Table 3). In the refinements of the La and Nd compounds, we fixed a statistical distribution of nitrogen and oxygen in the available anion sites because the X-rays do not provide enough contrast between the two anions. Attempts to refine a model with the larger cell of $a = 8.15$ and $c = 24.99$ Å observed by electron diffraction led to chemically inconsistent bond distances and
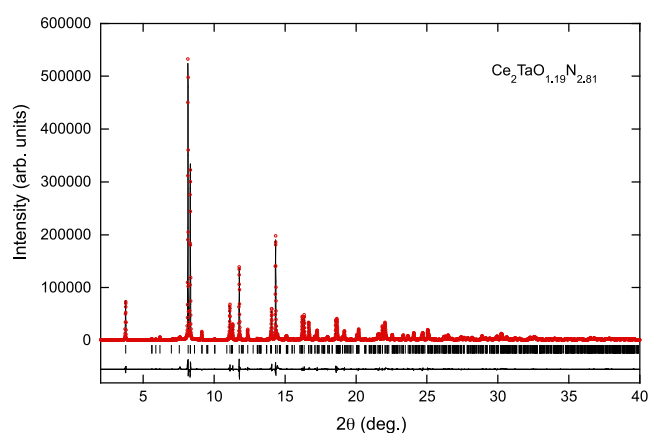
Figure 4. Rietveld fit to the synchrotron X-ray powder diffraction pattern of $Ce_2TaO_{1.19}N_{2.81}$ performed in the space group *Pccn* with cell parameters $a = 5.70500(5)$, $b = 5.71182(4)$, and $c = 12.61280(7)$ Å.

Figure 5. Rietveld fit to the synchrotron X-ray powder diffraction pattern of $Nd_2TaO_{1.46}N_{2.54}$ performed in the space group *Pccn* with cell parameters $a = 5.70466(3)$, $b = 5.70475(5)$, and $c = 12.32366(5)$ Å. Upper and lower reflection markers are, respectively, for $Nd_2TaO_{1.46}N_{2.54}$ and $NdTaON_2$.

angles. In the $I4_1/acd$ model, the doubling of the c_0 parameter results from a sequence of tilts along the c axis (θ tilts) that repeats every four layers of octahedra (Figure 8).[31] The cell volume of this compound normalized to a $\sqrt{2}a_0 \times \sqrt{2}a_0 \times c_0$ cell is 408.805 Å³, that is larger than for $Nd_2TaO_{1.46}N_{2.54}$

$(401.056(4)$ Å³) as a consequence of the divalent state of Eu^{2+}, with a larger ionic radius than that of Nd^{3+} (for CN = IX, $r(Eu^{2+}) = 1.30$ Å and $r(Nd^{3+}) = 1.163$ Å).[34] The cell volumes of the La (419.580(4) Å³) and Ce (411.000(5) Å³) compounds are significantly larger than for the Nd phase, as expected from the ionic radii of R^{3+} cations.[34] The Goldschmidt tolerance factors (t) for the four phases have been calculated from the ionic radii considering the formal compositions $La_2^{3+}Ta_{0.31}^{4+}Ta_{0.69}^{5+}O_{1.31}N_{2.69}$, $Ce_2^{3+}Ta_{0.19}^{4+}Ta_{0.81}^{5+}O_{1.19}N_{2.81}$, $Nd_2^{3+}Ta_{0.46}^{4+}Ta_{0.54}^{5+}O_{1.46}N_{2.54}$, and $Eu_{1.80}^{2+}Eu_{0.20}^{3+}TaO_{2.80}N_{1.20}$, leading to the values of 0.904 (La), 0.896 (Ce), 0.886 (Nd), and 0.930 (Eu), respectively. The larger t of the europium compound, together with the lower nitride content of this phase and an expected distinct anion ordering (see the next section), may account for its different crystal symmetry compared with the other rare earth derivatives.

Neutron Diffraction Study of $Ce_2TaO_{1.19}N_{2.81}$: Anion Order and the Prediction of Pauling's Second Crystal Rule in $n = 1$ Ruddlesden–Popper Oxynitrides. The refinement of neutron diffraction data of $Ce_2TaO_{1.19}N_{2.81}$ (Figure 9) was performed starting with a random distribution of nitrogen and oxygen in the three anion positions of the *Pccn* model, considering full occupancy in all sites and constraining the total content of each anion to the composition determined by chemical analysis. The refined N/O populations for the two equatorial sites were 93/7 (X2) and 88/12 (X3), whereas the obtained occupancies of the axial site X1 were 50% for each anion (Figure 6 and Table 4). This anion distribution shows a near-100% order of the nitride anions at the equatorial sites of the tantalum octahedra. The bond distances for these positions were significantly shorter ($d(Ta-X2) = 2.0504(3)$ Å, $d(Ta-X3) = 2.0346(2)$ Å) than for the axial site ($d(Ta-X1) = 2.1855(19)$ Å). The elongation of the octahedra along the c direction is an indication of the observed anion order, as the axial sites are occupied by 50% O/50% N, and the covalent character of metal–oxygen bonds is lower than for metal–nitrogen bonds. The large thermal parameter observed for the axial site is indicative of the O/N disorder in this position (see Figure 6). Shorter bond M–N distances compared to M–O bonds have been also observed in the hexagonal perovskite $BaWON_2$ [12] that shows the total order of N and O in corner-sharing positions and face-sharing positions of the W^{6+} octahedra. The observed anion order in $Ce_2TaO_{1.19}N_{2.81}$ is different from that previously reported in $n = 1$ Ruddlesden–Popper oxynitrides as a

Table 1. Summary of the *Pccn* Model Refined against Room-Temperature Synchrotron Powder X-ray Diffraction Data for $La_2TaO_{1.31}N_{2.69}$ ($\lambda = 0.4137$ Å)[a,b]

atom	site	x	y	z	B (Å²)	occupancy
La	8e	0.4965(7)	0.0043(6)	0.1419(5)	0.735(14)	1
Ta	4a	0	0	0	1.000(18)	1
O1/N1	8e	0.0185(13)	0.0600(6)	0.16527(18)	0.401(16)	0.33/0.67
O2/N2	4c	0.25	0.25	0.4761(5)	0.401	0.33/0.67
O3/N3	4d	0.25	0.75	−0.0065(4)	0.401	0.33/0.67

bond	d (Å)	bond	d (Å)	bond	d (Å)
Ta–O1,N1	2.142(2) × 2	Ta–O2,N2	2.049(1) × 2	Ta–O3,N3	2.0276(2) × 2
La–O1,N1	2.495(3)	La–O1,N1	2.516(5)	La–O1,N1	2.773(8)
La–O1,N1	3.023(8)	La–O1,N1	3.249(5)	La–O2,N2	2.551(5)
La–O2,N2	2.910(5)	La–O3,N3	2.662(4)	La–O3,N3	2.778(4)

[a]Refined cell parameters and agreement factors are $a = 5.72949(2)$, $b = 5.73055(5)$, and $c = 12.77917(6)$ Å. $V = 419.580(4)$ Å³. $R_{Bragg} = 3.46\%$ and $R_{wp} = 7.16\%$. [b]The O/N occupancies were fixed to a statistical distribution considering the chemical analysis. The temperature factors were common for the three anions sites. Average bond distances: Ta–O,N 2.073 Å and La–O,N 2.773 Å.
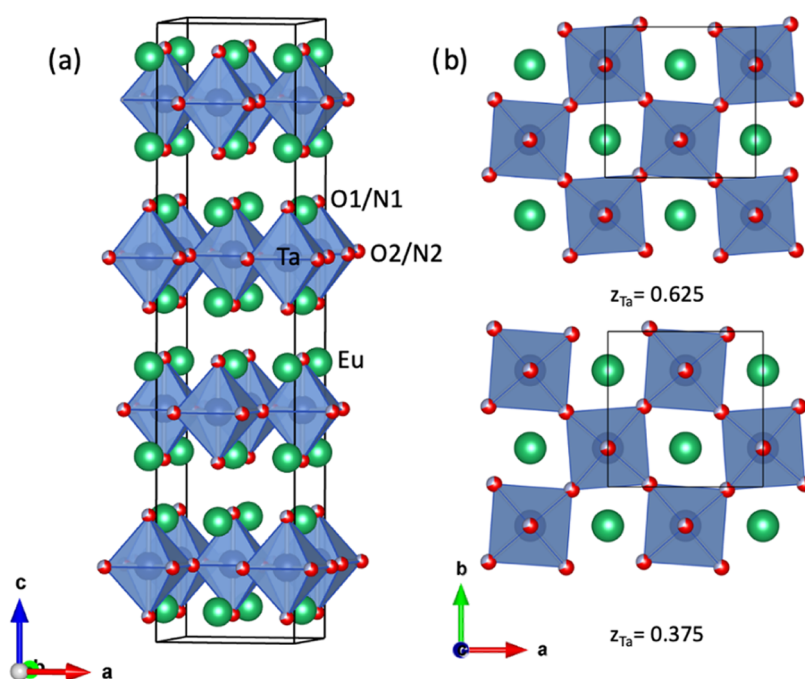
Table 2. Summary of the *Pccn* Model Refined against Room-Temperature Synchrotron X-ray Powder Diffraction Data for Nd$_2$TaO$_{1.46}$N$_{2.54}$ (λ = 0.4139 Å)^{a,b}

atom	site	x	y	z	B (Å^2)	occupancy
Nd	8e	0.5118(4)	−0.00580(8)	0.14307(3)	0.868(2)	1
Ta	4a	0	0	0	1.039(10)	1
O1/N1	8e	−0.047(4)	−0.049(4)	0.1774(7)	1.41(13)	0.37/0.63
O2/N2	4c	0.25	0.25	0.5277(7)	1.41	0.37/0.63
O3/N3	4d	0.25	0.75	−0.013(3)	1.41	0.37/0.63

bond	d (Å)	bond	d (Å)	bond	d (Å)
Ta−O1,N1	2.220(9) × 2	Ta−O2,N2	2.046(3) × 2	Ta−O3,N3	2.023(3)(×2)
Nd−O1,N1	2.259(10)	Nd−O1,N1	2.56(2)	Nd−O1,N1	2.58(2)
Nd−O1,N1	3.20(3)	Nd−O1,N1	3.23(3)	Nd−O2,N2	2.526(12)
Nd−O2,N2	2.866(15)	Nd−O3,N3	2.56(2)	Nd−O3,N3	2.81(3)

^{a}Refined cell parameters and agreement factors: a = 5.70466(3), b = 5.70475(5), and c = 12.32365(5) Å. V = 401.056(4) Å^3. R_{Bragg} = 4.74% and R_{wp} = 9.19%. ^{b}The O/N occupancies were fixed to a statistical distribution considering the chemical analysis. The temperature factors were common for the three anions sites. Average bond distances: Ta−O,N 2.096 Å and Nd−O,N 2.732 Å.
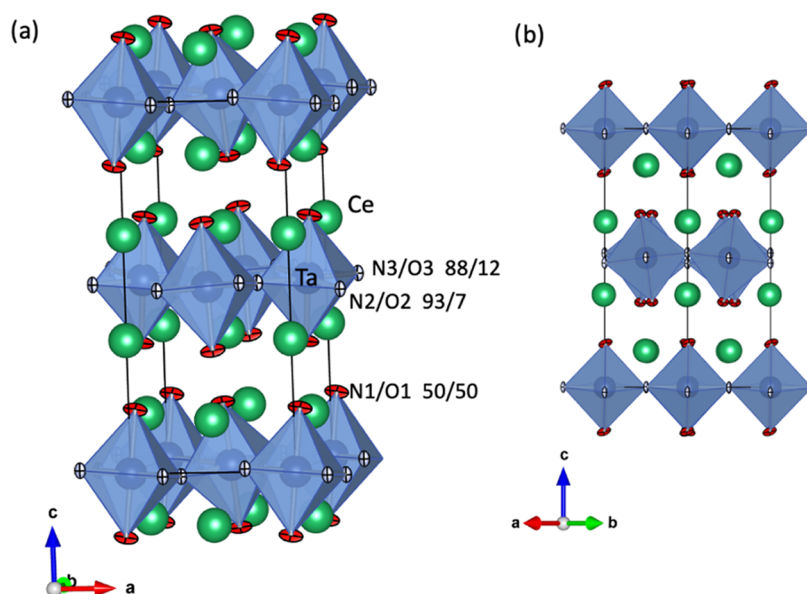
Figure 6. (a) Crystal structure of Ce$_2$TaO$_{1.19}$N$_{2.81}$ determined from neutron powder diffraction data. Thermal ellipsoids of the anions are shown at 50% probability. The refined N/O population (%) is indicated for each anion site. (b) Projection along 110 showing the tilting of the Ta octahedra.
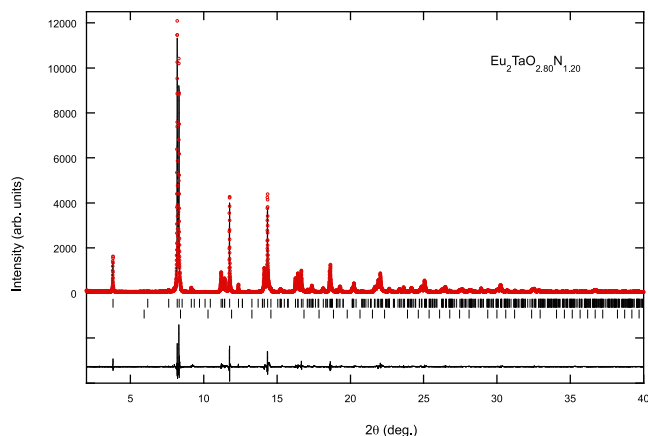
Figure 7. Rietveld fit to the synchrotron X-ray powder diffraction pattern of Eu$_2$TaO$_{2.80}$N$_{1.20}$ performed in the space group $I4_1/acd$ with cell parameters a = 5.71867(2) and c = 25.00092(19) Å. Upper and lower reflection markers are, respectively, for Eu$_2$TaO$_{2.80}$N$_{1.20}$ and EuTaO$_2$N, respectively.

consequence of its larger nitrogen content and higher charge of the A cation. In the less nitrided alkaline earth compounds Sr$_2$TaO$_3$N,[35,36] Ba$_2$TaO$_3$N,[36] and Sr$_2$NbO$_3$N[37] crystallizing in the $I4/mmm$ space group, the nitride anions also prefer the equatorial sites of the octahedra, but the N/O population for these positions is 50/50, whereas the axial sites are fully occupied by oxygen. These anion distributions agree with the prediction of Pauling's second crystal rule (PSCR),[38,39] which states that the electric charge of each anion (q) tends to compensate the strength of the electrostatic valence bonds from the cations, according to the equation $b = \sum_i \frac{z_i}{\nu_i}$, where z_i is the electric charge of each cation bonded to a given anionic position and ν_i is its coordination number. The b values for the equatorial and axial positions in A$_2$BO$_3$N compounds (A = Sr^{2+}, Ba^{2+}; B = Nb^{5+}, Ta^{5+}) are 2.55 and 1.94, respectively, in close agreement with the charge of the anions occupying these sites (q = −2.5 and −2)[37,39] using the determined distributions from neutron diffraction. For ideal R$_2$TaON$_3$ compounds, the trivalent rare earth cations increase the calculated sums for the equatorial and axial sites to 3 and 2.5, respectively. In Ce$_2$TaO$_{1.19}$N$_{2.81}$, considering 19% of Ta^{4+} and 81% of Ta^{5+}, the calculated sums

Figure 8. (a) Crystal structure of $Eu_2TaO_{2.80}N_{1.20}$ determined from synchrotron powder X-ray diffraction data. The nitride and oxide anions are depicted as gray and red spheres, respectively, and are distributed statistically in the X1 and X2 sites with proportions according to the chemical analysis. (b) Projection along c of the two central layers of the unit cell, showing the tilting of the Ta octahedra.

Table 3. Summary of the $I4_1/acd$ Model Refined against Room-Temperature Synchrotron X-ray Powder Diffraction Data for $Eu_2TaO_{2.80}N_{1.20}$ (λ = 0.4142 Å)[a,b]

atom	site	x	y	z	B (Å²)	occupancy
Eu	16d	0	0.25	0.552190(18)	0.686(10)	1
Ta	8a	0	0.25	0.375	0.922(15)	1
O1/N1	16d	0	0.25	0.4564(3)	2.816	0.70/0.30
O2/N2	16f	0.232(2)	0.482(2)	0.125	2.816	0.70/0.30

bond	d (Å)	bond	d (Å)
Ta−O1,N1	2.035(8) × 2	Ta−O2,N2	2.027(11) × 4
Eu−O1,N1	2.395(8)	Eu−O1,N1	2.867(1) × 4
Eu−O2,N2	2.830(9) × 2	Eu−O2,N2	2.614(8) × 2

[a]Refined cell parameters and agreement factors are a = 5.71867(2) and c = 25.00092(19) Å. V = 817.609(8) Å³. R_{Bragg} = 4.19% and R_{wp} = 10.5%. [b]Isotropic thermal parameters of the anions were fixed to 2.816 Å². O/N occupancies were fixed to a statistical distribution considering the chemical analysis. Average bond distances: Ta−O,N 2.030 Å and Eu−O,N 2.750 Å.
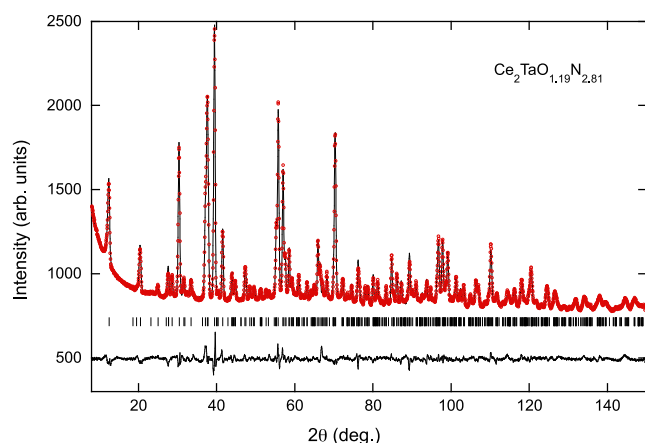
Figure 9. Rietveld fit to the neutron powder diffraction pattern of $Ce_2TaO_{1.19}N_{2.81}$ performed in the space group $Pccn$ with cell parameters a = 5.75284(19), b = 5.75620(15), and c = 12.71338(18) Å.

are 2.94 and 2.47 for the equatorial and axial sites, respectively, and the observed anion distribution leads to q = −2.93, − 2.88, and −2.5 for X2, X3, and X1 positions, respectively, in excellent agreement with the prediction of PSCR. A similar anion ordering can be expected for the other trivalent rare earth derivatives reported in this work, $La_2TaO_{1.31}N_{2.69}$ and $Nd_2TaO_{1.46}N_{2.54}$. However, for $Eu_2TaO_{2.80}N_{1.20}$, the PSCR-predicted distribution is the same as for the alkaline earth oxynitrides because the europium in this compound is essentially divalent, as the alkaline earth cations. Hence, the expected anion populations at the axial sites would be 50/50 for $La_2TaO_{1.31}N_{2.69}$ and $Nd_2TaO_{1.46}N_{2.54}$, whereas for $Eu_2TaO_{2.80}N_{1.20}$, 100% O occupancy is expected for the same positions. For the analyzed anion compositions in each compound, the expected populations at the equatorial sites would be, respectively, O/N 15/85, 23/77, and 40/60 for the La, Nd, and Eu compounds. Future neutron diffraction experiments are planned to corroborate these predictions.

Magnetic Properties. The Ce, Nd, and Eu compounds display a Curie-like paramagnetic susceptibility at high temper-

Table 4. Summary of the *Pccn* Model Refined against Room-Temperature Neutron Diffraction Data for Ce$_2$TaO$_{1.19}$N$_{2.81}$ (λ = 1.37 Å)^{a,b}

| atom	site	x	y	z	B (Å^2)	occupancy
Ce	8e	0.4997(17)	0.0115(8)	0.14118(15)	0.89(3)	1
Ta	4a	0	0	0	1.09(3)	1
O1/N1	8e	0.0309(11)	0.0401(5)	0.17037(13)	2.524	0.498(5)/0.502
O2/N2	4c	0.25	0.25	0.4800(2)	1.205	0.070(7)/0.930
O3/N3	4d	0.25	0.75	0.0011(11)	1.205	0.124(13)/0.876

bond	d (Å)	bond	d (Å)	bond	d (Å)
Ta-O1,N1	2.1855(19) × 2	Ta—O2,N2	2.0504(3) × 2	Ta—O3,N3	2.0346(2) × 2
Ce—O1,N1	2.421(3)	Ce—O1,N1	2.614(5)	Ce—O1,N1	2.727(12)
Ce—O1,N1	3.083(12)	Ce—O1,N1	3.202(5)	Ce—O2,N2	2.591(6)
Ce—O2,N2	2.854(6)	Ce—O3,N3	2.689(11)	Ce—O3,N3	2.739(11)

^{a}Refined cell parameters and agreement factors are a = 5.75284(19), b = 5.75620(15), and c = 12.71338(18) Å. V = 420.997(19) Å^3. R_{Bragg} = 5.22% and R_{wp} = 1.34%. ^{b}Estimated standard deviations in parentheses are shown once for each independent variable. The thermal parameters were refined anisotropically for the three anions; ellipsoids are shown on Figure 6. Average bond distances: Ta—O,N 2.090 Å and Ce—O,N 2.769 Å.
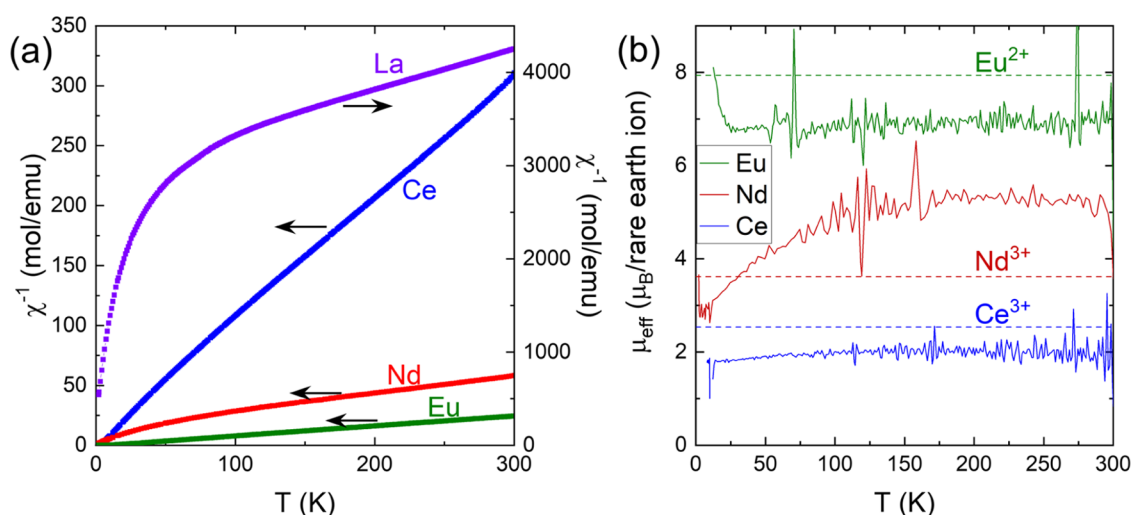
Figure 10. (a) Inverse susceptibility of La$_2$TaO$_{1.31}$N$_{2.69}$, Ce$_2$TaO$_{1.19}$N$_{2.81}$, Nd$_2$TaO$_{1.46}$N$_{2.54}$, and Eu$_2$TaO$_{2.80}$N$_{1.20}$, measured at 10 kOe (note the different scale, right axis, used for the La compound). (b) Temperature dependence of the effective paramagnetic moment obtained by the derivative of the inverse susceptibility as explained in the text.

ature (T > 50 K) (Figure 10a), although deviations are clearly perceptible at least in Nd$_2$TaO$_{1.46}$N$_{2.54}$, as typically found in rare earth compounds.[40] La$_2$TaO$_{1.31}$N$_{2.69}$ shows an extremely small paramagnetic susceptibility, in accordance with the non-magnetic nature of La^{3+} and plausibly associated with the presence of Ta^{4+} or to traces of magnetic impurity. A convenient way to identify deviations from the common Curie behavior and to get insights into their physical origin is to plot the effective paramagnetic moment (μ_{eff}), extracted from the measured susceptibility: $\chi_m = \mu_0 \frac{N_A \mu_B^2}{3k_B T} \mu_{eff}^2$. In Figure 10b, we show the μ_{eff} vs T plot, where μ_{eff} has been obtained through the thermal derivative of the inverse susceptibility: $\frac{d\chi_m^{-1}}{dT} = \frac{3k_B T}{N_A \mu_B^2 \mu_0} \frac{1}{\mu_{eff}^2}$. It turns out that for Eu and Ce compounds, μ_{eff} is temperature-independent down to about 25K. The observed effective moments approach, although slightly smaller, to those expected for Eu^{2+} ions (^{8}S$_{7/2}$; g_J = 2) and Ce^{3+} (^{2}F$_{5/2}$, g_J = 6/7) (green and blue dashed lines in Figure 10b), which may indicate some overoxidation of Eu^{2+} and Ce^{3+}. In fact, from the susceptibility of Ce$_2$TaO$_{1.19}$N$_{2.81}$, we infer an effective paramagnetic moment of $\mu_{eff} \simeq$ 2.02 μ_B/Ce, which could signal the partial appearance of Ce^{4+}(J = 0), estimated to be around 37%, together with an

accompanying fraction of Ta^{4+} (J = 1/2) for charge compensation. The presence of Ce^{4+} may be induced by the existence of nitrogen-rich regions created by the anion disorder, that will be balanced by oxide-rich regions where Ta^{5+} is reduced to Ta^{4+} according to the internal redox equilibrium Ce^{3+} + Ta^{5+} $\Leftrightarrow$ Ce^{4+} + Ta^{4+}.[4] The observed effective paramagnetic moment of Eu$_2$TaO$_{2.80}$N$_{1.20}$ is $\mu_{eff} \simeq$ 7.63 μ_B/Eu, which assuming a coexistence of Eu^{2+} and Eu^{3+} would correspond to a concentration of Eu^{3+} of about 10%, in excellent agreement with the chemical analysis. The small magnetic moment in the broad and rather delocalized 5d^1 orbitals of Ta^{4+} ions should lead to a minor contribution to the measured small susceptibility. In contrast, the Nd$_2$TaO$_{1.46}$N$_{2.54}$ compound displays a conspicuous decrease of μ_{eff} on cooling below $T \simeq$ 100 K. This is the common behavior of rare earths with an odd number of electrons in magnetically diluted systems, and it may result from crystal field effects or the presence of magnetic interactions, as discussed latter. For instance, the crystal field may break the degeneracy of the ground-state $^{2S+1}$L$_J$ of the rare earth into various site symmetry-dependent Kramers doublets, with electron occupancy, and thus, the magnetic susceptibility will evolve with temperature. The presence of magnetic interactions may also result in a reduction of magnetic
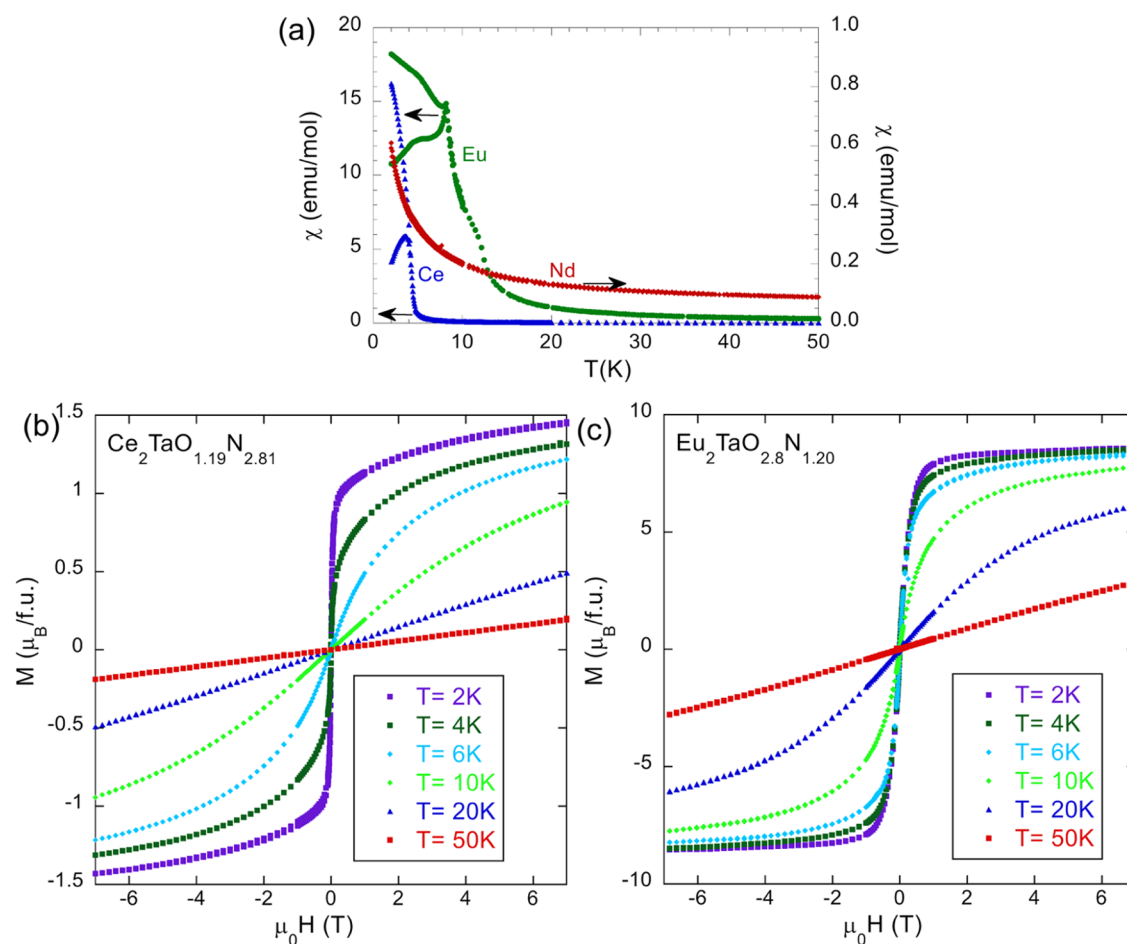
Figure 11. (a) Zero field-cooled/field-cooled magnetization vs temperature (measured under 25 Oe applied magnetic field) of $Nd_2TaO_{1.46}N_{2.54}$ (right axis) and $Ce_2TaO_{1.19}N_{2.81}$ and $Eu_2TaO_{2.80}N_{1.20}$ (left axis). (b, c) Magnetization vs magnetic field measured at different temperatures for $Ce_2TaO_{1.19}N_{2.81}$ and $Eu_2TaO_{2.80}N_{1.20}$, respectively.

susceptibility. It follows that the origin of the observed temperature dependence of $\mu_{eff}(T)$ cannot be, in general, univocally disentangled.[41] On the other hand, the observation that in the high-temperature limit, the measured μ_{eff} is larger than the free ion Nd^{3+} value ($^4I_{9/2}$; $J = 9/2$, $g_J = 8/11$) remains intriguing. It could be tentatively attributed to some spin polarization of neighboring Ta^{4+} ions, as in $Nd_2TaO_{1.46}N_{2.54}$, the proportion of this cation is the largest among the $R_2TaO_{4-x}N_x$ series presented here.

To get a deeper insight into the low-temperature spontaneous magnetic behavior of these compounds, we explored the low-field magnetic susceptibility (χ). In Figure 11a, we show $\chi(T)$ measured on heating under 25 Oe magnetic field after a zero-field cooling (ZFC) and field cooling (FC). A well-pronounced peak followed by a low-temperature hysteresis shows up in the ZFC-FC at ∼4K for $Ce_2TaO_{1.19}N_{2.81}$ and ∼8K for $Eu_2TaO_{2.80}N_{1.20}$, indicating the appearance of magnetic order in these compounds. In contrast, $Nd_2TaO_{1.46}N_{2.54}$ does not display any hysteresis and thus no traces of magnetic order down to the lowest explored temperature (2K). To understand the origin of this hysteresis, we have measured the field-dependent magnetization. The obtained $M(H)$ curves are depicted in Figure 11b,c. Data show a rapid upturn of magnetic moment under a low magnetic field at low temperatures characteristic of magnetic order with a ferromagnetic component. We have discarded that this upturn corresponds to a paramagnet at low

enough temperature by plotting the magnetization vs H/T and checked that the $M(H/T)$ curves at the lowest temperature ($T < 15$ K) do not scale (see Figure S3). Data collected at the lowest temperature reflect a lack of saturation, suggesting the coexistence of the remaining fraction of disordered spins in the samples.

The saturation magnetization (M_S) inferred from data collected at the lowest temperature (2K) and largest field (7 T) indicates $M_S(Ce_2TaO_{1.19}N_{2.81}) \sim 0.7 \ \mu_B/Ce$ and $M_S(Eu_2TaO_{2.80}N_{1.20}) \sim 4.3 \ \mu_B/Eu$. Both values are significantly smaller than those expected for fully collinear ferromagnetic orders: 2.14 μ_B/Ce for Ce^{3+} and 1.35 μ_B/Ce for the aforementioned 37% of Ce^{4+}; 7 μ_B/Eu for full Eu^{2+}, and 6.3 μ_B/Eu for 10% of Eu^{3+} (according to chemical analysis). This discrepancy between the expected (or the maximal) and observed values of the saturation magnetization indicates that a more complex ordering pattern could be at work or that the disorder in the system drives to magnetic frustration and to an only partially ordered magnetic structure.

At first sight, the lack of magnetic ordering in $Nd_2TaO_{1.46}N_{2.54}$ may seem surprising as structural differences between the Nd, Ce, and Eu compounds are rather small. For the rare earth cations in the K_2NiF_4-type structure, there are eight super-exchange pathways corresponding to the next nearest neighbors (NNN), four from the same NaCl-type layer (J_{21}) and four from a neighbor layer (J_{22}) (see Figure 12a−c).[42] In these pathways,
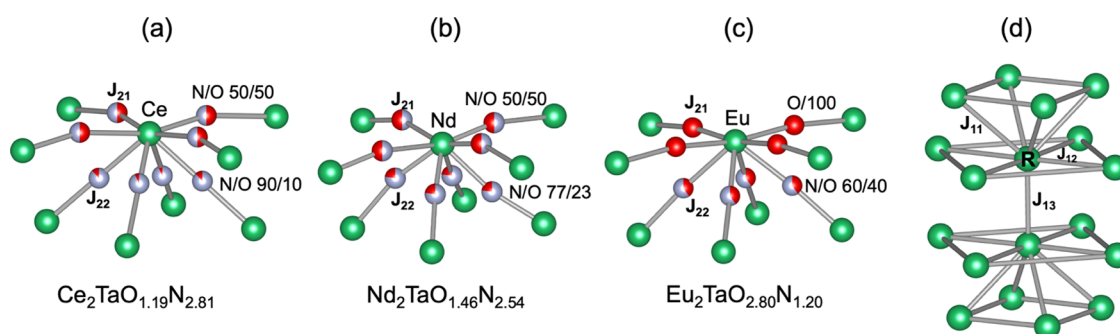
Figure 12. (a−c) Superexchange (J_{21}, J_{22}) and (d) direct exchange (J_{11}, J_{12}, J_{13}) magnetic interactions in $R_2TaO_{3-x}N_x$ compounds (R = Ce, Nd, Eu). Anion occupancies correspond to those determined from neutron diffraction for $Ce_2TaO_{1.19}N_{2.81}$. For $Nd_2TaO_{1.46}N_{2.54}$ and $Eu_2TaO_{2.80}N_{1.20}$, the anion populations are those expected using PSCR (see the precedent section).

the changes of bond distances across the series are extremely moderate ($\approx 1\%$), and the R−X−R bond angles change monotonically by $\approx 3\%$ (171.41° for the Eu compound, 167.7° for $Ce_2TaO_{1.19}N_{2.81}$ and 160.7° for $Nd_2TaO_{1.46}N_{2.54}$) (Figure 13). On the other hand, any superexchange R−X−R magnetic
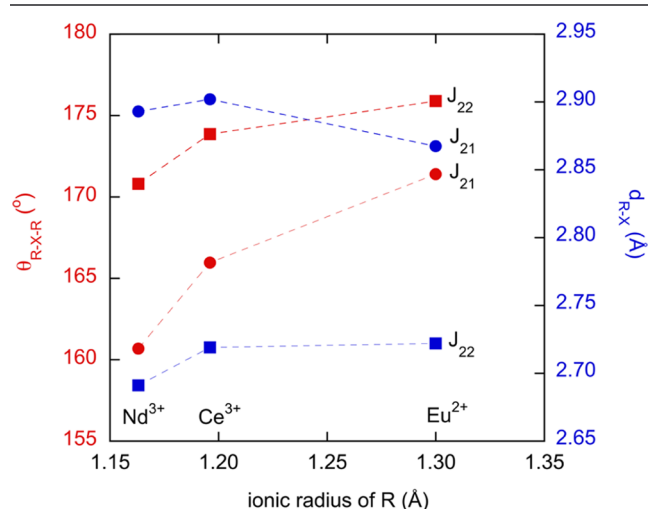
Figure 13. Average R−X−R angles and R−X (X = O,N) bond distances for superexchange interactions in $Ce_2TaO_{1.19}N_{2.81}$ (from neutron diffraction data), $Nd_2TaO_{1.46}N_{2.54}$, and $Eu_2TaO_{2.80}N_{1.20}$ plotted against the ionic radii of Ce^{3+}, Nd^{3+}, and Eu^{2+}, respectively, for CN = IX.[34]

interaction is expected to be stronger when increasing the covalency of bonds by reducing the electronegativity of the anions,[43] and thus, a larger N/O ratio will reinforce the superexchange interactions. As illustrated in Figure 12, the N/O occupancy in the R−X−R pathways for $Nd_2TaO_{1.46}N_{2.54}$ is similar to that of the Ce compound and larger than in the Eu compound, and still no magnetic order is observed in the Nd compound. From these two sets of data, we conclude that superexchange interactions do not appear to play a major role in the magnetic ordering of the rare earth ions in these compounds, which thus appear to be governed by direct R−R exchange interactions depicted in Figure 12d. In exchange-coupled Nd^{3+}-Nd^{3+} units, crystal field and exchange interactions conspicuously combine to produce a singlet ground state, which is in sharp contrast with Ce^{3+}-Ce^{3+} and Eu^{2+}-Eu^{2+}units where the ground state can be a triplet (see, for instance, Figures 31, 26, and 22, pages 64−69 in ref [40]). It follows that the effective magnetic moment of Nd^{3+} decreases when decreasing temperature, and no magnetic order develops in $Nd_2TaO_{1.46}N_{2.54}$, which is

completely different than the behavior of $Ce_2TaO_{1.19}N_{2.81}$ and $Eu_2TaO_{2.80}N_{1.20}$ compounds in agreement with our experimental observations.

CONCLUSIONS

The new $n = 1$ Ruddlesden−Popper rare earth tantalum oxynitrides $R_2TaO_{4-x}N_x$ (R = La, Ce, Nd, and Eu) are prepared using a solid-state reaction under N_2 at temperatures between 1200 and 1700 °C starting with mixtures of R_2O_3, RN, Ta_3N_5, and TaON. This is a versatile synthetic approach that allows to control the initial N/O ratio, a determining factor to stabilize the oxynitrides, by using different proportions of the four reactants while keeping the R/Ta = 2 stoichiometric ratio. The chemical analyses of the obtained oxynitrides $La_2TaO_{1.31}N_{2.69}$, $Ce_2TaO_{1.19}N_{2.81}$, $Nd_2TaO_{1.46}N_{2.54}$, and $Eu_2TaO_{2.80}N_{1.20}$ indicate a decrease of the N/O ratio during the synthesis that leads to an excess of oxygen with respect to the ideal stoichiometry R_2TaON_3, corresponding to the oxidation states of the cations R^{3+} and Ta^{5+}. The lower nitrogen content is formally charge-compensated by the reduction of europium to the divalent state or of Ta^{5+} to Ta^{4+}.

The La, Ce, and Nd compounds show a tilted superstructure with cell parameters $\sqrt{2}a_0 \times \sqrt{2}a_0 \times c_0$ (where a_0 and c_0 are the parameters of the $I4/mmm$ K_2NiF_4 aristotype) with the $Pccn$ space group. In contrast, the europium compound shows additional doubling of the c axis, with parameters $\sqrt{2}a_0 \times \sqrt{2}a_0 \times 2c_0$, and crystallizes in the $I4_1/acd$ space group. The observed different crystal chemistry in the europium compound is a consequence of the near total reduction of this rare earth to Eu^{2+}. The neutron diffraction study of $Ce_2TaO_{1.19}N_{2.81}$ shows that the equatorial sites of the tantalum octahedra have an occupancy of nearly 100% nitrogen, whereas the axial sites are occupied by 50% of each anion. This anion distribution is in excellent agreement with the prediction of Pauling's second crystal rule that leads to the bond strength sums of 2.94 and 2.47 for the equatorial and axial sites, respectively. According to this prediction, a similar anion order is expected for the trivalent rare earth $n = 1$ Ruddlesden−Popper oxynitrides of La and Nd. For the Eu^{2+} compound, the corresponding calculated sums are 2.55 and 1.94; hence, a population of 50/50 O/N in the equatorial sites and 100% O in the axial sites is predicted. The Ce and Eu compounds display some magnetic order at low temperatures with a ferromagnetic component. In contrast, the Nd oxynitride does not show any fingerprint of magnetic order but remains paramagnetic down to the lowest temperature explored (2 K), consistent with the temperature-independent effective magnetic moment observed in the former and a low-

temperature suppression in the latter, which we attribute to the combined effect of a temperature-dependent change of electron occupancy in the crystal-field split Kramers doublets and exchange interactions producing a singlet ground state. The new $n = 1$ Ruddlesden−Popper compounds reported in this paper expand the structural diversity of the family of perovskite oxynitrides opening avenues to search new materials in this group of solids. Post-treatments of the $R_2TaO_{4-x}N_x$ samples in strongly nitriding atmospheres such as NH_3 would plausibly increase the nitrogen contents with concomitant oxidation of the cations Eu^{2+} and Ta^{4+}, and new applications as dielectric materials or as visible light photocatalysts in different reactions may emerge.

■ ASSOCIATED CONTENT

Ⓢ Supporting Information

The Supporting Information is available free of charge at https://pubs.acs.org/doi/10.1021/acs.chemmater.4c00533.

> Electron diffraction patterns of $La_2TaO_{1.31}N_{2.69}$ and $Nd_2TaO_{1.46}N_{2.54}$, refinement of synchrotron X-ray powder diffraction data of $Ce_2TaO_{1.19}N_{2.81}$, and magnetization vs μ_0H/T curves of $Ce_2TaO_{1.19}N_{2.81}$ and $Eu_2TaO_{2.80}N_{1.20}$ (PDF)

■ AUTHOR INFORMATION

Corresponding Authors

Josep Fontcuberta − *Institut de Ciència de Materials de Barcelona (ICMAB-CSIC), 08193 Bellaterra, Spain;* Email: fontcuberta@icmab.cat

Amparo Fuertes − *Institut de Ciència de Materials de Barcelona (ICMAB-CSIC), 08193 Bellaterra, Spain;* ⓞ orcid.org/0000-0001-5338-9724; Email: amparo.fuertes@icmab.es

Authors

Jhonatan R. Guarín − *Institut de Ciència de Materials de Barcelona (ICMAB-CSIC), 08193 Bellaterra, Spain*

Carlos Frontera − *Institut de Ciència de Materials de Barcelona (ICMAB-CSIC), 08193 Bellaterra, Spain;* ⓞ orcid.org/0000-0002-0091-4756

Judith Oró-Solé − *Institut de Ciència de Materials de Barcelona (ICMAB-CSIC), 08193 Bellaterra, Spain*

Bastian Colombel − *Institut de Ciència de Materials de Barcelona (ICMAB-CSIC), 08193 Bellaterra, Spain*

Clemens Ritter − *Institut Laue-Langevin, F-38042 Grenoble Cedex 9, France*

François Fauth − *CELLS-ALBA Synchrotron, Barcelona 08290, Spain;* ⓞ orcid.org/0000-0001-9465-3106

Complete contact information is available at:
https://pubs.acs.org/10.1021/acs.chemmater.4c00533

Author Contributions

The article was written through contributions of all authors. All authors have given approval to the final version of the article.

Notes

The authors declare no competing financial interest.

■ REFERENCES

(1) Fuertes, A. Nitride Tuning of Transition Metal Perovskites. *APL Mater.* **2020**, *8*, No. 020903.

(2) Jansen, M.; Letschert, H. P. Inorganic Yellow-Red Pigments without Toxic Metals. *Nature* **2000**, *404*, 980−982.

(3) Jorge, A. B.; Oró-Solé, J.; Bea, A. M.; Mufti, N.; Palstra, T. T. M.; Rodgers, J. A.; Attfield, J. P.; Fuertes, A. Large Coupled Magneto-responses in EuNbO₂N. *J. Am. Chem. Soc.* **2008**, *130*, 12572−12573.

(4) Yang, M.; Oró-Solé, J.; Kusmartseva, A.; Fuertes, A.; Attfield, J. P. Electronic Tuning of Two Metals and Colossal Magnetoresistances in EuWO₁₊ₓN₂₋ₓ Perovskites. *J. Am. Chem. Soc.* **2010**, *132*, 4822−4829.

(5) Kim, Y.-I.; Woodward, P. M.; Baba-Kishi, K. Z.; Tai, C. W. Characterization of the Structural, Optical, and Dielectric Properties of Oxynitride Perovskites AMO₂N (A = Ba, Sr, Ca; M = Ta, Nb). *Chem. Mater.* **2004**, *16*, 1267−1276.

(6) Wang, Q.; Domen, K. Particulate Photocatalysts for Light-Driven Water Splitting: Mechanisms, Challenges, and Design Strategies. *Chem. Rev.* **2020**, *120*, 919−985.

(7) Chen, K.; Xiao, J.; Vequizo, J. M.; Hisatomi, T.; Ma, Y.; Nakabayashi, M.; Takata, T.; Yamakata, A.; Shibata, N.; Domen, K. Overall Water Splitting by a SrTaO₂N-Based Photocatalyst Decorated with an Ir-Promoted Ru-Based Cocatalyst. *J. Am. Chem. Soc.* **2023**, *145*, 3839−3843.

(8) Ceravola, R.; Frontera, C.; Oró-Solé, J.; Black, A. P.; Ritter, C.; Mata, I.; Molins, E.; Fontcuberta, J.; Fuertes, A. Topochemical Nitridation of Sr₂FeMoO₆. *Chem. Commun.* **2019**, *55*, 3105−3108.

(9) Ceravola, R.; Oró-Solé, J.; Black, A. P.; Ritter, C.; Puente Orench, I.; Mata, I.; Molins, E.; Frontera, C.; Fuertes, A. Topochemical Synthesis of Cation Ordered Double Perovskite Oxynitrides. *Dalton Trans.* **2017**, *46*, 5128−52131.

(10) Ishida, K.; Tassel, C.; Watabe, D.; Takatsu, H.; Brown, C. M.; Nilsen, G. J.; Kageyama, H. Spin Frustration in Double Perovskite Oxides and Oxynitrides: Enhanced Frustration in La₂MnTaO₅N with a Large Octahedral Rotation. *Inorg. Chem.* **2021**, *60*, 8252−8258.

(11) Guarín, J. R.; Frontera, C.; Oró-Solé, J.; Gàzquez, J.; Ritter, C.; Fontcuberta, J. Fuertes. High-Temperature Synthesis of Ferromagnetic Eu₃Ta₃(O,N)₉ with a Triple Perovskite Structure. *Inorg. Chem.* **2023**, *62*, 17362−17370.

(12) Oró-Solé, J.; Fina, I.; Frontera, C.; Gàzquez, J.; Ritter, C.; Cunquero, M.; Loza-Alvarez, P.; Conejeros, S.; Alemany, P.; Canadell, E.; Fontcuberta, J.; Fuertes, A. Engineering Polar Oxynitrides: Hexagonal Perovskite BaWON₂. *Angew. Chem., Int. Ed.* **2020**, *59*, 18395−18399.

(13) Ruddlesden, S. N.; Popper, P. New Compounds of the K₂NiF₄ type. *Acta Crystallogr.* **1957**, *10*, 538−539.

(14) Pors, F.; Marchand, R.; Laurent, Y. Nouveaux Oxynitrures A₂TaO₃N (A = Alcalinoterreux) de type structural K₂NiF₄. *Ann. Chim. Fr.* **1991**, *16*, 547−551.

(15) Marchand, R. Oxynitrures à Structure K$_2$NiF$_4$. Les composés Ln$_2$AlO$_3$N (Ln = La, Nd, Sm). *C.R. Acad. Sci. Paris* **1976**, *282*, 329–331.

(16) Tobías, G.; Oró-Solé, J.; Beltrán-Porter, D.; Fuertes, A. New Family of Ruddlesden-Popper Strontium Niobium Oxynitrides: (SrO)(SrNbO$_{2-x}$N)$_n$ (n = 1, 2). *Inorg. Chem.* **2001**, *40*, 6867–6869.

(17) Cordes, N.; Nentwig, M.; Eisenburger, L.; Oeckler, O.; Schnick, W. Ammonothermal Synthesis of the Mixed-Valence Nitrogen-Rich Europium Tantalum Ruddlesden-Popper Phase Eu^{II}Eu$_2^{III}$Ta$_2$N$_4$O$_3$. *Eur. J. Inorg. Chem.* **2019**, *2019*, 2304–2311.

(18) Black, A. P.; Johnston, H. E.; Oró-Solé, J.; Bozzo, B.; Ritter, C.; Frontera, C.; Attfield, J. P.; Fuertes, A. Nitride Tuning of Lanthanide Chromites. *Chem. Commun.* **2016**, *52*, 4317–4320.

(19) Oró-Solé, J.; Clark, L.; Kumar, N.; Bonin, W.; Sundaresan, A.; Attfield, J. P.; Rao, C. N. R.; Fuertes, A. Synthesis, Anion Order and Magnetic Properties of RVO$_{3-x}$N$_x$ Perovskites (R = La, Pr, Nd; 0 ≤ x ≤ 1). *J. Mater. Chem.* **2014**, *C2*, 2212–2220.

(20) Kasahara, A.; Nukumizu, K.; Hitoki, G.; Takata, T.; Kondo, J. N.; Hara, M.; Kobayashi, H.; Domen, K. Photoreactions on LaTiO$_2$N under Visible Light Irradiation. *J. Phys. Chem. A* **2002**, *106*, 6750–6753.

(21) Black, A. P.; Suzuki, H.; Higashi, M.; Frontera, C.; Ritter, C.; De, C.; Sundaresan, A.; Abe, R.; Fuertes, A. New Rare Earth Hafnium Oxynitride Perovskites with Photocatalytic Activity in Water Oxidation and Reduction. *Chem. Commun.* **2018**, *54*, 1525–1528.

(22) Wang, X.; Hisatomi, T.; Wang, Z.; Song, J.; Qu, J.; Takata, T.; Domen, K. Core–Shell-Structured LaTaON$_2$ Transformed from LaKNaTaO$_5$ Plates for Enhanced Photocatalytic H$_2$ Evolution. *Angew. Chem., Int. Ed.* **2019**, *58*, 10666–11070.

(23) Castets, A.; Fina, I.; Guarín, J. R.; Oró-Solé, J.; Frontera, C.; Ritter, C.; Fontcuberta, J.; Fuertes, A. High-Temperature Synthesis and Dielectric Properties of LaTaON$_2$. *Inorg. Chem.* **2021**, *60*, 6484–16491.

(24) Fauth, F.; Peral, I.; Popescu, C.; Knapp, M. The New Material Science Powder Diffraction Beamline at ALBA Synchrotron. *Powder Diffr.* **2013**, *28*, S360–S370.

(25) Rodríguez-Carvajal, J. Recent Advances in Magnetic Structure Determination by Neutron Powder Diffraction. *Phys. B* **1993**, *192*, 55–69.

(26) Fuertes, A. Synthetic Approaches in Oxynitride Chemistry. *Prog. Sol. State Chem.* **2018**, *51*, 63–70.

(27) Kawashima, K.; Hojamberdiev, M.; Wagata, H.; Yubuta, K.; Vequizo, J. J. M.; Yamakata, A.; et al. NH3-assisted flux-mediated direct growth of LaTiO$_2$N crystallites for visible light-induced water splitting. *J. Phys. Chem. C* **2015**, *119*, 15896–15904.

(28) Yang, M.; Rodgers, J. A.; Middler, L. C.; Oró-Solé, J.; Jorge, A. B.; Fuertes, A.; Attfield, J. P. Direct Solid State Synthesis at High Pressures of New Mixed-Metal oxynitrides: RZrO$_2$N (R = Pr, Nd and Sm). *Inorg. Chem.* **2009**, *48*, 11498–11500.

(29) Chen, D.; Habu, D.; Masubuchi, Y.; Torii, S.; Kamiyama, T.; Kikkawa, S. Partial Nitrogen Loss in SrTaO$_2$N and LaTiO$_2$N Oxynitride Perovskites. *Solid State Sci.* **2016**, *54*, 2–6.

(30) Cox, P. A. *Transition Metal Oxides: An Introduction to Their Electronic Structure and Properties*; Clarendon Press: Oxford, 1995.

(31) Liu, T.; Holzapfel, N. P.; Woodward, P. M. Understanding structural distortions in hybrid layered perovskites with the n = 1 Ruddlesden–Popper structure. *IUCrJ.* **2023**, *10*, 385–396.

(32) Aleksandrov, K. S.; Beznosikov, B. V.; Misyul, S. V. Successive Structure Phase-Transitions in Crystals of K$_2$MgF$_4$-Type Structure. *Phys. Status Solidi* **1987**, *104*, 529–543.

(33) Shimura, T.; Inaguma, Y.; Nakamura, T.; Itoh, M.; Morii, Y. Structure and magnetic properties of Sr$_{2-x}$A$_x$IrO$_4$ (A = Ca, Ba). *Phys. Rev. B* **1995**, *52*, 9143–9146.

(34) Shannon, R. D. Revised Effective Ionic Radii and Systematic Studies of Interatomic Distances in Halides and Chalcogenides. *Acta Crystallogr. A* **1976**, *32*, 751–767.

(35) Diot, N.; Marchand, R.; Haines, J.; Léger, J. M.; Macaudière, P.; Hull, S. Crystal Structure Determination of the Oxynitride Sr$_2$TaO$_3$N. *J. Solid State Chem.* **1999**, *146*, 390–393.

(36) Clarke, S. J.; Hardstone, K. A.; Michie, C. W.; Rosseinsky, M. J. High-Temperature Synthesis and Structures of Perovskite and n = 1 Ruddlesden–Popper Tantalum Oxynitrides. *Chem. Mater.* **2002**, *14*, 2664–2669.

(37) Tobías, G.; Beltrán-Porter, D.; Lebedev, O.; Van Tendeloo, G.; Rodríguez-Carvajal, J.; Fuertes, A. Anion Ordering and Defect Structure in Ruddlesden-Popper Strontium Niobium Oxynitrides. *Inorg. Chem.* **2004**, *43*, 8010–8017.

(38) Pauling, L. The Principles Determining the Structure of Complex Ionic Crystals. *J. Am. Chem. Soc.* **1929**, *51*, 1010–1026.

(39) Fuertes, A. Prediction of Anion Distributions Using Pauling's Second Rule. *Inorg. Chem.* **2006**, *45*, 9640–9642.

(40) Lueken, H. *Course of Lectures on Magnetism of Lanthanide Ions Under Varying Ligand and Magnetic Fields*; RWTH Aachen University, 2008.

(41) Kahn, M. L.; Sutter, J.-P.; Golhen, S.; Guionneau, P.; Ouahab, L.; Kahn, O.; Chasseau, D. Systematic Investigation of the Nature of The Coupling between a Ln(III) Ion (Ln = Ce(III) to Dy(III)) and Its Aminoxyl Radical Ligands. Structural and Magnetic Characteristics of a Series of {Ln(organic radical)$_2$} Compounds and the Related {Ln(Nitrone)$_2$} Derivatives. *J. Am. Chem. Soc.* **2000**, *122*, 3413–3421.

(42) Chien, C.-L.; DeBenedetti, S.; Barros, F. D. S. Magnetic properties of EuTiO$_3$, Eu$_2$TiO$_4$ and Eu$_3$Ti$_2$O$_7$. *Phys. Rev. B* **1974**, *10*, 3913–3922.

(43) Trócoli, R.; Frontera, C.; Oró-Solé, J.; Ritter, C.; Alemany, P.; Canadell, E.; Palacín, M. R.; Fontcuberta, J.; Fuertes, A. MnTa$_2$N$_4$: A Ternary Nitride Spinel with a Strong Magnetic Frustration. *Chem. Mater.* **2022**, *34*, 6098–6107.